arXiv:1201.6556v1 [astro-ph.SR] 31 Jan 2012

HS 2325+8205 - an ideal laboratory for accretion disc physics

S. Pyrzas[1], B. T. Gänsicke[1], J. R. Thorstensen[2], A. Aungwerojwit[3,4], D. Boyd[5], S. Brady[6],
J. Casares[7,8], R. D. G. Hickman[1], T. R. Marsh[1], I. Miller[9], Y. Ögmen[10], J. Pietz[11],
G. Poyner[12], P. Rodríguez-Gil[7,8], B. Staels[13]

ABSTRACT

We identify HS 2325+8205 as an eclipsing, frequently outbursting dwarf nova with an orbital period of $P_{\rm orb} = 279.841731(5)$ min. Spectroscopic observations are used to derive the radial velocity curve of the secondary star from absorption features and also from the Hα emission lines, originating from the accretion disc, yielding $K_{\rm sec} = K_{\rm abs} = 237 \pm 28\,{\rm km\,s^{-1}}$ and $K_{\rm em} = 145 \pm 9\,{\rm km\,s^{-1}}$ respectively. The distance to the system is calculated to be $400(+200, -140)$ pc. A photometric monitoring campaign reveals an outburst recurrence time of $\sim 12 - 14$ d. The combination of magnitude range ($17 - 14$ mag), high declination, eclipsing nature and frequency of outbursts makes HS 2325+8205 the ideal system for "real-time" studies of the accretion disc evolution and behaviour in dwarf nova outbursts.

---

[1] Department of Physics, University of Warwick, Coventry, CV4 7AL, UK

[2] Department of Physics and Astronomy, 6127 Wilder Laboratory, Dartmouth College, Hanover, NH 03755, USA

[3] Department of Physics, Faculty of Science, Naresuan University, Phitsanulok, 65000, Thailand

[4] ThEP Center, CHE, 328 Si Ayutthaya Road, Bangkok, 10400, Thailand

[5] British Astronomical Association, Variable Star Section, West Challow OX12 9TX, UK

[6] AAVSO, 25 Birch Street, Cambridge, MA 02138, USA

[7] Instituto de Astrofísica de Canarias, Vía Láctea, s/n, La Laguna, E-38205, Tenerife, Spain

[8] Departamento de Astrofísica, Universidad de La Laguna, E-38206 La Laguna, Tenerife, Spain

[9] British Astronomical Association, Variable Star Section, Furzehill House, Ilston, Swansea SA2 7LE, UK

[10] Green Island Observatory, Geçitkale, Mugosa, via Mersin 10, Cyprus

[11] Nollenweg 6, 65510 Idstein, Germany

[12] British Astronomical Association, Variable Star Section, 67 Ellerton Road, Kingstanding, Birmingham B44 0QE, UK

[13] CBA Flanders, Alan Guth Observatory, Koningshofbaan 51, Hofstade, Aalst, Belgium

Subject headings: stars

1. Introduction

Dwarf novae are a sub-class of non- (or weakly) magnetic cataclysmic variables (CVs, see e.g. Warner 1995, for a comprehensive review), in which a white dwarf primary accretes matter via an accretion disc, formed by material transferred through the L_1 point from a Roche lobe-filling (near) main-sequence secondary. The defining trait of dwarf novae are quasi-periodical brightness changes of several magnitudes, commonly known as "dwarf nova outbursts". It is widely accepted that outbursts can be understood within the framework of the disc instability model (DIM, see e.g. Smak 1984; Cannizzo 1993; Osaki 1996; Lasota 2001, for reviews of the topic). Within DIM accretion discs undergo outbursts if the mass transfer rate is below a critical value, $\dot{M}_{\rm crit}$. Above the CV orbital period gap[1] accretion rates are usually larger than $\dot{M}_{\rm crit}$ and, as a result, only about a third of non-magnetic systems are dwarf novae. The situation is completely different below the period gap, where dwarf novae dominate the CV population (Shafter 1992).

Dwarf novae provide the best environment to develop and test our understanding of accretion disc structure and dynamics, which is relevant to a wide range of objects, such as low-mass X-ray binaries (LMXBs, Dubus et al. 2001), active galactic nuclei (AGN, Burderi et al. 1998) and young stellar objects (YSO, Bell & Lin 1994).

Of particular interest in this context are eclipsing dwarf novae. In these systems, the physical properties of the binary, such as the mass ratio, the inclination angle, the masses and temperatures of the component stars and the radial structure of the accretion disc can be determined to high precision, through studies of the eclipse features of the white dwarf, the bright spot (formed in the region where the mass-transferring stream meets the accretion disc) and accretion disc components (see e.g. Wood et al. 1989; Littlefair et al. 2006b; Southworth et al. 2009).

HS 2325+8205 (RA: $23^{\rm h}$ $26^{\rm min}$ $50.4^{\rm s}$, Dec: +82° 22' 12" [J2000], henceforth HS 2325) was one of the systems identified in a dedicated search for CVs (Aungwerojwit et al. 2005) within the Hamburg Quasar Survey (HQS, Hagen et al. 1995)). Photometric observations soon revealed the eclipsing nature of the system and also frequently occuring outbursts. An interesting historic note is that Morgenroth (1936) mentioned short-term variability of HS 2325, which correspondingly was included in the New Catalogue of Suspected Variable

---

[1] The orbital period range $2\,{\rm h} \leq P_{\rm orb} \leq 3\,{\rm h}$, where only a small number of CVs are found.

Stars as NSV 14581 (though with rather uncertain coordinates).

2. Observations

We obtained photometric and spectroscopic data on HS 2325 using both large aperture ($>$ 1m) and small aperture telescopes. Table 1 summarizes the observations conducted with the former. A brief account on data reduction follows.

2.1. Photometry

We obtained time-series photometry of HS 2325 during 17 nights throughout the period 2003 to 2007 using 1.2–2.5 m telescopes (Table 1). These observations were reduced with the pipeline described in Gänsicke et al. (2004), which employs bias-subtraction and flat-fielding in the standard fashion within MIDAS and uses SEXTRACTOR (Bertin & Arnouts 1996) to perform aperture photometry. Sample light curves are shown in Fig. 1.

HS 2325 has been found to vary in brightness between $\sim 17^{th}$ and $\sim 14^{th}$ magnitude. Eclipses are shallow and maintain an almost constant depth, during the rise to outburst. The eclipses in the bright state exhibit a symmetric U-shape, typical for an accretion disc-dominated system. During quiescence the eclipse morphology becomes more complicated and reveals several breaks in slope. In addition to eclipses, the light curve of HS 2325 displays two further features: short-term, random, out-of-eclipse variations, known as “flickering” (e.g. Bruch 2000), and an “orbital hump”, a brightening just before the start of the eclipse attributed to the bright spot coming into view (e.g. Krzeminski 1965).

An intensive 1.5-month-long photometric campaign was conducted in 2009 to characterise the outburst behaviour of HS 2325, using small aperture (11”-14”) telescopes. The data were reduced with AIP4WIN and MAXIMDL, and the resulting light curve is shown in Fig. 2.

2.2. Spectroscopy

Spectroscopic observations during the system’s quiescence were obtained at the 2.4m Hiltner telescope at MDM Observatory on Kitt Peak, Arizona. The modular spectrograph and a SiTe 2048^2 pixel CCD yielded 2 Å/pixel and from 4210 to 7500 Å but with decreased sensitivity toward the ends of the wavelength range. The spectral resolution was $\sim$ 3.5 Å full width at half maximum (FWHM). Reductions were performed mostly with standard `IRAF` routines, but we used an original implementation of the optimal extraction algorithm detailed by Horne (1986) to compute one-dimensional spectra from the two-dimensional images. For wavelength calibration, we used a dispersion curve derived from lamp exposures in twilight, and corrected for nighttime drifts using the $\lambda\,5577$ sky line. We observed standard stars in twilight whenever the sky appeared clear, and used these observations to flux-calibrate the data. The scatter of the standard stars typically suggests that the flux calibration is uncertain by several tenths of a magnitude, probably due to uncalibrated losses at the spectrograph slit. The mean quiescent spectrum is shown in Fig. 3. The flux level of the observed spectrum implies a V-band magnitude near 17.0, subject to the calibration uncertainties.

3. Orbital Period and Ephemeris

Mid-eclipse times (given in Table 2) were determined by visually cross-correlating each eclipse profile with its mirror image with respect to time. This was found to produce more robust results than fitting a parabola to the eclipse minimum, in particular for the light curves with poor time resolution. We adopted the duty cycle (exposure plus readout time) of the corresponding observations as a conservative estimate of the uncertainty in the mid-eclipse times.

Fitting a linear ephemeris to the mid-eclipse times gives

$$T_0(\mathrm{HJD}) \;=\; 2\,452\,888.42554(3) \;+\; 0.194\,334\,535(3)\,\mathrm{E} \tag{1}$$

with mid-eclipse times calculated on a UTC timescale, i.e. an orbital period of $P_{\mathrm{orb}} = 279.841731(5)$ min.

4. Secondary spectral type and radial velocities analysis

As is typical for quiescent dwarf novae, the Balmer lines in emission are the most prominent features in the spectrum of HS 2325 with equivalent widths of $\simeq 30$ and $\simeq 54$ Å for Hβ and Hα respectively. He I emission is detected at 4921, 5015, and 5876 Å, and Fe II $\lambda5169$ as well (the features at $\lambda\lambda$ 4921 and 5015 may also be blended with Fe II). The absorption bands of an M-dwarf companion are conspicuous. To quantify the M dwarf contribution, we subtracted library spectra of M dwarfs classified by Boeshaar (1976), taken with the same instrument, and varied the spectral type and scaling until the M-dwarf features were cancelled as well as possible. The lower two traces in Fig. 3 show the decomposition that was (at least subjectively) the best. From this exercise, we estimate that the companion is of type M3.0 ± 0.75 subclasses, and that its flux corresponds to $V = 19.0 \pm 0.4$ (external error, including calibration uncertainties). The spectral type-period relation of Smith & Dhillon (1998) (Equation 4 in their paper) for $\mathrm{P} > 4\,\mathrm{h}$ yields Sp2 = M1.5 for the derived orbital period of $P_{\rm orb} = 4.664\,\mathrm{h}$, a value broadly consistent with our estimate of M3.0 ± 0.75, as the rms scatter of the spectral type-period relation is 3 subtypes for $\mathrm{P} > 4\,\mathrm{h}$ (Smith & Dhillon 1998).

We measured radial velocities of the Hα emission line using a double-Gaussian convolution method outlined by Schneider & Young (1980); the centres of the Gaussians were separated by $1280\,\mathrm{km\,s^{-1}}$, and each individual Gaussian had a FWHM of $270\,\mathrm{km\,s^{-1}}$, comparable to our spectral resolution. This emphasised the outer wings of the line profile. We also tried a range of separations, and found that the radial velocity amplitude and phase were insensitive to this parameter. To measure the velocity of the M-dwarf component, we used the cross-correlation program `rvsao`, written by Kurtz & Mink (1998). For the template, we used a velocity-compensated composite M-dwarf spectrum, composed by summing the spectra of a large number of M dwarfs for which Marcy et al. (1987) tabulate precise velocities. The cross-correlation region was from 6000 to 6500 Å; this was chosen to include some strong atomic and TiO features, while avoiding emission lines. Not all the spectra gave usable cross-correlation velocities; we limited our analysis to those for which the formal velocity error was less than $35\,\mathrm{km\,s^{-1}}$.

We then performed fits to the radial velocities (both absorption and Hα emission), of the form $v(t) = \gamma + K \sin[(t - T_0)\,/\,P_{\rm orb}]$. The orbital period $P_{\rm orb}$ was held fixed to the value derived from eclipses. Because of the modest number of absorption velocities and their limited phase coverage, and because the absorption should trace the motion of the secondary star fairly well, we fixed T_0 to the mid-eclipse ephemeris when fitting the absorption velocities, but left it as a free parameter for the Hα emission ones. The resulting velocities were $K_{\rm sec} = K_{\rm abs} = 237(28)\,\mathrm{km\,s^{-1}}$, $\gamma_{\rm abs} = -19(20)\,\mathrm{km\,s^{-1}}$, $K_{\rm em} = 145(9)\,\mathrm{km\,s^{-1}}$, $\gamma_{\rm em} = -42(6)\,\mathrm{km\,s^{-1}}$ for the absorption and emission lines respectively, with the numbers in parentheses indicating the errors. Figure 4 shows the emission and absorption velocities as a function of orbital phase, while Fig. 5 shows a greyscale representation of the low-state spectra, as a function of phase. The upper panel of Fig. 5 is scaled to emphasize the M-dwarf absorption features, and to show the structure in the HeI λ5876 line; the orbital motion of the M dwarf is clearly seen. The scaling of the lower panel brings out the complex structure in the Hα emission.

5. Distance

We can estimate the distance to HS 2325 using the secondary star's contribution to the spectrum and our knowledge of the orbital period $P_{\rm orb}$. For a secondary star of mass $M_{\rm sec}$ at a fixed $P_{\rm orb}$, the Roche lobe radius R_2 is proportional to ${M_{\rm sec}}^{1/3}$, and is almost independent of the primary mass $M_{\rm WD}$ (Beuermann et al. 1998). We do not know $M_{\rm sec}$, but we can estimate it using evolutionary models tabulated by Baraffe & Kolb (2000); these suggest that the secondary is between 0.23 and 0.56 $\rm M_\odot$. At this $P_{\rm orb}$, Eq. 1 of Beuermann et al. (1998) then implies $R_2 = 0.47 \pm 0.07\,\rm R_\odot$. Beuermann et al. (1999) tabulate absolute magnitudes and radii for late type dwarfs as a function of spectral class, which implies a surface brightness for each star. In the range of spectral type we see here, these correspond to $M_V = 8.8 \pm 0.7$ for a $1\rm R_\odot$ star, where the uncertainty includes both the spectral type uncertainty and the scatter among the tabulated points. Combining this with the radius yields an estimate of $M_V = 10.4 \pm 0.8$ for the secondary. The Galactic coordinates of HS 2325 are $(l, b) = (120°, 20°)$; at this location, Schlegel et al. (1998) estimate $E(B-V) = 0.19$ to the edge of the Galaxy. Assuming that our object lies outside most of the dust, and taking the M-dwarf contribution to the spectrum as $V = 19.0 \pm 0.4$, then yields an extinction-corrected distance modulus of $(m-M)_0 = 8.0 \pm 0.9$, corresponding to a distance of 400(+200, −140) pc. Note carefully that this estimate makes no assumption that the secondary follows a main-sequence mass-radius relation; it assumes only that the secondary's spectral type is a reliable guide to its surface brightness, and that it fills its Roche lobe.

6. Outburst behaviour

We intensively monitored HS 2325 for about 50 days, starting from the 1st of April 2009 using small aperture telescopes. Four outbursts have been recorded during this period, indicating a recurrence time of $\sim\ 12-14\,$d. Prominent in Fig. 2 is a "long" outburst, lasting $\sim 11-12\,$d, followed by a seemingly "short" outburst. This could be a hint towards a bimodal distribution of the outburst duration, observed in many dwarf novae (see e.g. Szkody & Mattei 1984; Ak et al. 2002). Further observations are required to establish a more accurate recurrence time and to check the consistency of the "long" and "short" outburst succession.

We have inspected v7.12 (2009) of the Ritter and Kolb catalogue (Ritter & Kolb 2003) and compiled a list of U Gem-type dwarf novae (UG) and Z Cam-type stars (ZC) that are found in the range $4\,{\rm h} < P_{\rm orb} < 5\,{\rm h}$. Only systems with confirmed UG/ZC status and with a quoted outburst recurrence period were considered. This left us with a list of 22 systems (out of the 39 listed in R&K in this $P_{\rm orb}$ range). In this list ZC systems dominate the short end of the outburst recurrence period distribution ($11-18$ d), while UG systems tend to have longer intervals between outbursts ($16-150$ d). Our inferred outburst recurrence period places HS 2325 in the ZC region. However, as there has been no recorded standstill (the hallmark of ZC systems), its identification as either a UG or a ZC remains ambiguous.

7. Estimates of the binary properties

The standard treatment of eclipsing CVs (see e.g. Wood et al. 1986, 1992; Littlefair et al. 2006a) involves the identification of the contact points of the white dwarf, the bright spot and the accretion disc. The corresponding phase-widths are then used to place firm (geometrical) constraints on the mass ratio q and the inclination angle i (e.g. Bailey 1979; Horne 1985) and deduce information about the extend and location of the bright spot and the size of the accretion disc. Flickering can hinder attempts to identify the contact points. Averaging together many light curves is an often applied solution (see e.g. Copperwheat et al. 2010, for the case of IP Peg).

Although breaks in slope are seen in the light curve of HS 2325, the available data set is not of sufficient quality and time-resolution to unambiguously identify the different contact points. Hence, the exact eclipse geometry of HS 2325 remains unclear.

In an attempt to constrain the parameter space (albeit roughly) we have to rely on theoretical predictions and empirical evidence from the observed CV population, coupled with the limited information that can be extracted from the light curves.

Following the procedure outlined in detail in Dhillon et al. (1991) (D91) the radius of the accretion disc can be determined as a function of the binary separation, q and i, for a given eclipse half-width at maximum intensity $\Delta\phi$ (essentially timing the first and last contacts of eclipse and dividing by two). $\Delta\phi$ was determined by eye to be $\Delta\phi = 0.1 \pm 0.02$. The large error is due to the fact that the exact beginning and end of the eclipse are uncertain because of flickering.

The left panel of Fig. 6 shows the disc radius $R_{\rm D}$ (in units of the distance between the primary and the inner Lagrangian point, R_{L_1}) calculated using Equations 3, 4 and 5 of D91, for $0 \leq q \leq 1$ and various inclination angles. The curves are bound above by the requirement that $R_{\rm D} \leq R_{L_1}$ and below by the requirement for a partial disc eclipse, satisfied if the disc radius is larger than the half-cord of the secondary (shown by the change in line colour in the left panel of Fig. 6). This allows us to place a strict lower limit for the inclination angle to be $i_{\rm min} = 68°$. However, the upper limit of i and the possible values of q remain unconstrained.

Using the mass function,

$$f\left(M_{\rm WD}\right) = \frac{\left(M_{\rm WD}\sin i\right)^3}{\left(M_{\rm WD}+M_{\rm sec}\right)^2} = \frac{P_{\rm orb}K_{\rm sec}^3}{2\pi G} \quad \leq M_{\rm WD} \tag{2}$$

we can transform a given (q, i) pair to a unique $(M_{\rm WD}, M_{\rm sec})$ pair. The right panel of Figure 6 shows Eq. 2 calculated for $i_{\rm min} = 68°$ and $i_{\rm max} = 90°$, over a wide range in secondary mass, $0.1 \leq M_{\rm sec}\,[{\rm M}_\odot] \leq 0.6$. Allowed $(M_{\rm WD}, M_{\rm sec})$ pairs are located between the two dash-dot curves.

We can further narrow down the parameter space, by making two assumptions:

1. The secondary follows the mass-period relation of Smith & Dhillon (1998); their Equation 8 (power-law fit) yields $M_{\rm sec} = 0.43 \pm 0.07\,{\rm M}_\odot$, while their Equation 9 (linear fit) yields $M_{\rm sec} = 0.48 \pm 0.07\,{\rm M}_\odot$ (Fig. 6, right panel, dashed horizontal lines). An average of these values is in perfect agreement with the value of $M_{\rm sec} = 0.45\,{\rm M}_\odot$ predicted by the revised model track of Knigge et al. (2011) for this orbital period.
2. The radial velocity variation of the emission lines tracks the motion of the white dwarf, so $K_{\rm em} = K_{\rm WD} = 145 \pm 9\,{\rm km\,s^{-1}}$ and, therefore, $q = K_{\rm WD}/K_{\rm sec} = 0.61 \pm 0.08$ (Fig. 6, right panel, dotted lines).

While the latter is a frequently adopted assumption in CV research, it has to be viewed with a certain amount of caution, see e.g. Shafter (1983) and Thorstensen (2000). An encouraging fact in the case of HS 2325 is that the phasing of the emission lines is consistent with the eclipse ephemeris. The constraint on q imposes a narrower range of inclination angles $70° \leq i \leq 81°$ (Fig. 6, left panel, dashed vertical lines). If these assumptions are indeed correct, then the allowed $(M_{\rm WD}, M_{\rm sec})$ pairs are indicated as the grey shaded area in the right panel of Fig. 6.

8. Discussion and Conclusions

In this paper, we identified HS 2325+8205 as an eclipsing, frequently outbursting dwarf nova above the CV orbital period gap and presented our photometric and spectroscopic data. We used these data to measure the orbital period and the radial velocity of the secondary star, as well as provide initial estimates on the binary parameters. With the photometric data at hand it remains unclear whether the white dwarf is fully eclipsed or not. The shallow eclipse depth could suggest that it is not eclipsed at all. High time resolution and signal-to-noise data at quiescence are needed in order to unambigously identify the eclipse geometry.

The short outburst cycle of $\sim 12-14$ d makes HS 2325 a plausible Z Cam-type candidate. If confirmed, it will be only the third known eclipsing Z Cam system, after EM Cyg (e.g. North et al. 2000, and references therein) and AY Psc (e.g. Gülsecen et al. 2009, and references therein).

HS 2325, with its high declination (circumpolar, ideal for observers in the northern hemisphere), short outburst recurrence period and magnitude range (accessible with 2-4m class telescopes) offers an excellent target for systematic follow-up observations. Simultaneous high-time resolution photometric and spectroscopic observations can provide unique insight in the changes in the structure of the accretion disc, through techniques such as eclipse mapping (Horne 1985) and Doppler tomography (Marsh & Horne 1988).

Furthermore, the outbursts of HS 2325 can be picked-up with relative ease by small aperture telescopes enabling the accumulation of a very long baseline of outburst data, which can then be compared to the predictions of the disc instability model. We strongly encourage observers from around the world to frequently monitor the system and put the Z Cam-type scenario to the test.

JRT gratefully acknowledges support from the U.S. National Science Foundation, through grants AST-0307413 and AST-0708810. Based in part on observations made with the Nordic Optical Telescope, operated on the island of La Palma jointly by Denmark, Finland, Iceland, Norway, and Sweden, in the Spanish Observatorio del Roque de los Muchachos of the Instituto de Astrofísica de Canarias; on observations collected at the Centro Astronómico Hispano Alemán (CAHA) at Calar Alto, operated jointly by the Max-Planck Institut für Astronomie and the Instituto de Astrofísica de Andalucía (CSIC); on observations made at the 1.2m telescope, located at Kryoneri Korinthias, and owned by the National Observatory of Athens, Greece; and on observations obtained at the MDM Observatory, operated by Dartmouth College, Columbia University, Ohio State University, and the University of Michigan.

REFERENCES

Ak, T., Ozkan, M. T., Mattei, J. A., 2002, A&A, 389, 478

Aungwerojwit, A., et al., 2005, A&A, 443, 995

Bailey, J., 1979, MNRAS, 187, 645

Baraffe, I., Kolb, U., 2000, MNRAS, 318, 354

Bell, K. R., Lin, D. N. C., 1994, ApJ, 427, 987

Bertin, E. & Arnouts, S. 1996, A&AS, 117, 393

Beuermann, K., Baraffe, I., Kolb, U., Weichhold, M., 1998, A&A, 339, 518

Beuermann, K., Baraffe, I., Hauschildt, P., 1999, A&A, 348, 524

Boeshaar, P. C., 1976, The spectral classification of M-dwarf stars, Ph.D. thesis, Ohio State Univ., Columbus.

Bruch, A., 2000, A&A, 359, 998

Burderi, L., King, A. R., Szuszkiewicz, E., 1998, ApJ, 509, 85

Cannizzo, J. K., 1993, Accretion Disks in Compact Stellar Systems, ed. Wheeler, J. C. (Singapore: World Scientific), 6

Copperwheat, C. M., Marsh, T. R., Dhillon, V. S., Littlefair, S. P., Hickman, R., Gänsicke, B. T., Southworth, J., 2010, MNRAS, 402, 1824

Dhillon, V. S., Marsh, T. R., Jones, D. H. P., 1991, MNRAS, 252, 342

Dubus, G., Hameury, J.-M., Lasota, J.-P., 2001, A&A, 373, 251

Gänsicke, B. T., Araujo-Betancor, S., Hagen, H.-J., Harlaftis, E. T., Kitsionas, S., Dreizler, S., Engels, D., 2004, A&A, 418, 265

Gülsecen, H., Retter, A., Liu, A., Esenoğlu, H., 2009, New Astronomy, 14, 330

Hagen, H.-J., Groote, D., Engels, D., Reimers, D., 1995, A&AS, 111, 195

Horne, K., 1985, MNRAS, 213, 129

Horne, K., 1986, PASP, 98, 609

Knigge, C., Baraffe, I., Patterson, J., 2011, ApJS, 194, 28

Krzeminski, W., 1965, ApJ, 142, 1051

Kurtz, M. J., Mink, D. J., 1998, PASP, 110, 934

Lasota, J.-P., 2001, New Astronomy Review, 45, 449

Littlefair, S. P., Dhillon, V. S., Marsh, T. R., Gänsicke, B. T., 2006a, MNRAS, 371, 1435

Littlefair, S. P., Dhillon, V. S., Marsh, T. R., Gänsicke, B. T., Southworth, J., Watson, C. A., 2006b, Science, 314, 1578

Marcy, G. W., Lindsay, V., Wilson, K., 1987, PASP, 99, 490

Marsh, T. R., Horne, K., 1988, MNRAS, 235, 269

Morgenroth, O., 1936, Astronomische Nachrichten, 258, 265

North, R. C., Marsh, T. R., Moran, C. K. J., Kolb, U., Smith, R. C., Stehle, R., 2000, MNRAS, 313, 383

Osaki, Y., 1996, PASP, 108, 39

Ritter, H., Kolb, U., 2003, A&A, 404, 301

Schlegel, D. J., Finkbeiner, D. P., Davis, M., 1998, ApJ, 500, 525

Schneider, D. P., Young, P., 1980, ApJ, 238, 946

Shafter, A. W., 1983, ApJ, 267, 222

Shafter, A. W., 1992, ApJ, 394, 268

Smak, J., 1984, PASP, 96, 5

Smith, D. A., Dhillon, V. S., 1998, MNRAS, 301, 767

Southworth, J., Hickman, R. D. G., Marsh, T. R., Rebassa-Mansergas, A., Gänsicke, B. T., Copperwheat, C. M., Rodríguez-Gil, P., 2009, A&A, 507, 929

Szkody, P., Mattei, J. A., 1984, PASP, 96, 988

Thorstensen, J. R., 2000, PASP, 112, 1269

Warner, B., 1995, Cataclysmic Variable Stars, Cambridge University Press, Cambridge

Wood, J., Horne, K., Berriman, G., Wade, R., O'Donoghue, D., Warner, B., 1986, MNRAS, 219, 629

Wood, J. H., Horne, K., Berriman, G., Wade, R. A., 1989, ApJ, 341, 974

Wood, J. H., Horne, K., Vennes, S., 1992, ApJ, 385, 294

This preprint was prepared with the AAS LaTeX macros v5.2.

Table 1. Log of the observations with large aperture (> 1m) telescopes. Given is the run ID, the date of observation, the start and end of observation in HJD, the telescope and the filter (photometry) or grating (spectroscopy) used. “Frames” denotes the number of frames collected, “Ecl” the number of eclipses observed, “Mag” the out-of-eclipse magnitude and “Depth” the eclipse depth in magnitudes. Information about the telescopes and instruments used is provided at the bottom of the Table.

ID	Date	HJD range[a]	Telescope	Filter/Grating	Exp. time [s]	Frames	Ecl.	Mag.	Depth [mag]
01	2003 Sep 05	2888.255 - 2888.518	KY[b]	clear	30	646	1	14.9	0.4
02	2004 Jun 10	3167.429 - 3167.467	KY	clear	30	90	0	15.1	-
03	2004 Jun 11	3168.413 - 3168.593	KY	clear	30	390	1	15.7	0.8
04	2004 Jun 12	3169.451 - 3169.569	KY	clear	30	270	0	16.1	-
05	2004 Jul 25	3212.455 - 3212.607	KY	clear	30	389	1	16.0	0.8
06	2004 Jul 27	3214.298 - 3214.573	KY	clear	30	693	2	16.2	0.8
07	2004 Oct 21	3300.212 - 3300.493	KY	clear	20	997	2	16.4	0.8
08	2004 Oct 22	3301.213 - 3301.478	KY	clear	20	897	1	15.9	0.7
09	2004 Oct 23	3302.214 - 3302.457	KY	clear	20	858	1	14.6	0.4
10	2005 Sep 05	3619.333 - 3619.546	CA22[c]	clear	10	572	1	14.4	0.4
11	2005 Sep 11	3624.727 - 3624.804	HT[d]	600 l/mm	360/480	17	-	-	-
12	2005 Sep 12	3625.649 - 3625.909	HT	600 l/mm	360/480	31	-	-	-
13	2005 Sep 15	3629.599 - 3629.668	NOT[e]	clear	4	564	1	17	0.7
14	2005 Sep 16	3630.550 - 3630.715	NOT	clear	4	1308	1	16.5	0.6
15	2006 Aug 23	3971.321 - 3971.621	KY	clear	30	727	1	14.5	0.4
16	2006 Oct 28	4037.248 - 4037.504	KY	clear	30	595	1	16.3	0.8
17	2007 Jan 24	4124.604 - 4124.610	HT	600 l/mm	360/480	2	-	-	-

[a] Start to end of observation, in the format HJD - 2450000.

[b] 1.2m Kryoneri telescope (KY), CCD SI-502, 516 x 516, FOV 2.5′ x 2.5′

[c] 2.2m Calar Alto telescope (CA22), CAFOS, CCD SITe 2k x 2k, FOV 16′ x 16′

[d] 2.4m Hiltner Telescope (HT), CCD SiTe 2k x 2k

[e] 2.5m Nordic Optical Telescope (NOT), ALFOSC, CCD EEV42-40 2k x 2k, FOV 6.5′ x 6.5′

Table 2. Mid-eclipse times and their errors, the difference between observed and computed eclipse times and the cycle number using the ephemeris provided in Eq. 1. Times are calculated on a UTC timescale and given in the format HJD − 2450000.

T_0 [HJD]	Error [HJD]	O-C [s]	Cycle	T_0 [HJD]	Error [HJD]	O-C [s]	Cycle	T_0 [HJD]	Error [HJD]	O-C [s]	Cycle
2888.425480	0.000405	-6	0	4320.476770	0.000463	3	7369	4940.598350	0.000463	10	10560
3168.461560	0.000405	-4	1441	4335.440630	0.000463	12	7446	4941.375690	0.000775	10	10564
3212.575440	0.000405	-9	1668	4358.371920	0.000463	-4	7564	4941.569840	0.000463	-6	10565
3214.324580	0.000405	2	1677	4379.360110	0.000463	1	7672	4942.347170	0.001157	-7	10569
3214.518890	0.000405	-0	1678	4393.352210	0.000463	2	7744	4942.541460	0.000463	-11	10570
3300.220510	0.000289	7	2119	4451.458200	0.000810	-1	8043	4943.513250	0.001157	-0	10575
3300.414840	0.000289	7	2120	4510.535910	0.000463	0	8347	4944.485020	0.001157	8	10580
3301.386470	0.000289	3	2125	4524.527990	0.000810	-1	8419	4945.456530	0.001157	-6	10585
3302.357990	0.000289	-10	2130	4544.544400	0.000463	-5	8522	4945.650900	0.000660	-3	10586
3619.512060	0.000231	-1	3762	4560.479940	0.000810	5	8604	4945.845190	0.000660	-7	10587
3629.617580	0.000116	10	3814	4927.383490	0.000775	0	1049	4946.428210	0.001157	-6	10590
3630.589230	0.000116	8	3819	4933.602120	0.000810	-6	1052	4947.399870	0.000775	-7	10595
3971.452040	0.000405	11	5573	4934.573920	0.000810	4	1052	4948.371720	0.000660	8	10600
4037.331340	0.000405	2	5912	4935.351320	0.000775	10	1053	4963.529620	0.000810	-8	10678
4289.577510	0.000463	-3	7210	4935.545640	0.001007	8	1053	4964.695730	0.000810	0	10684
4312.508950	0.000463	-6	7328								

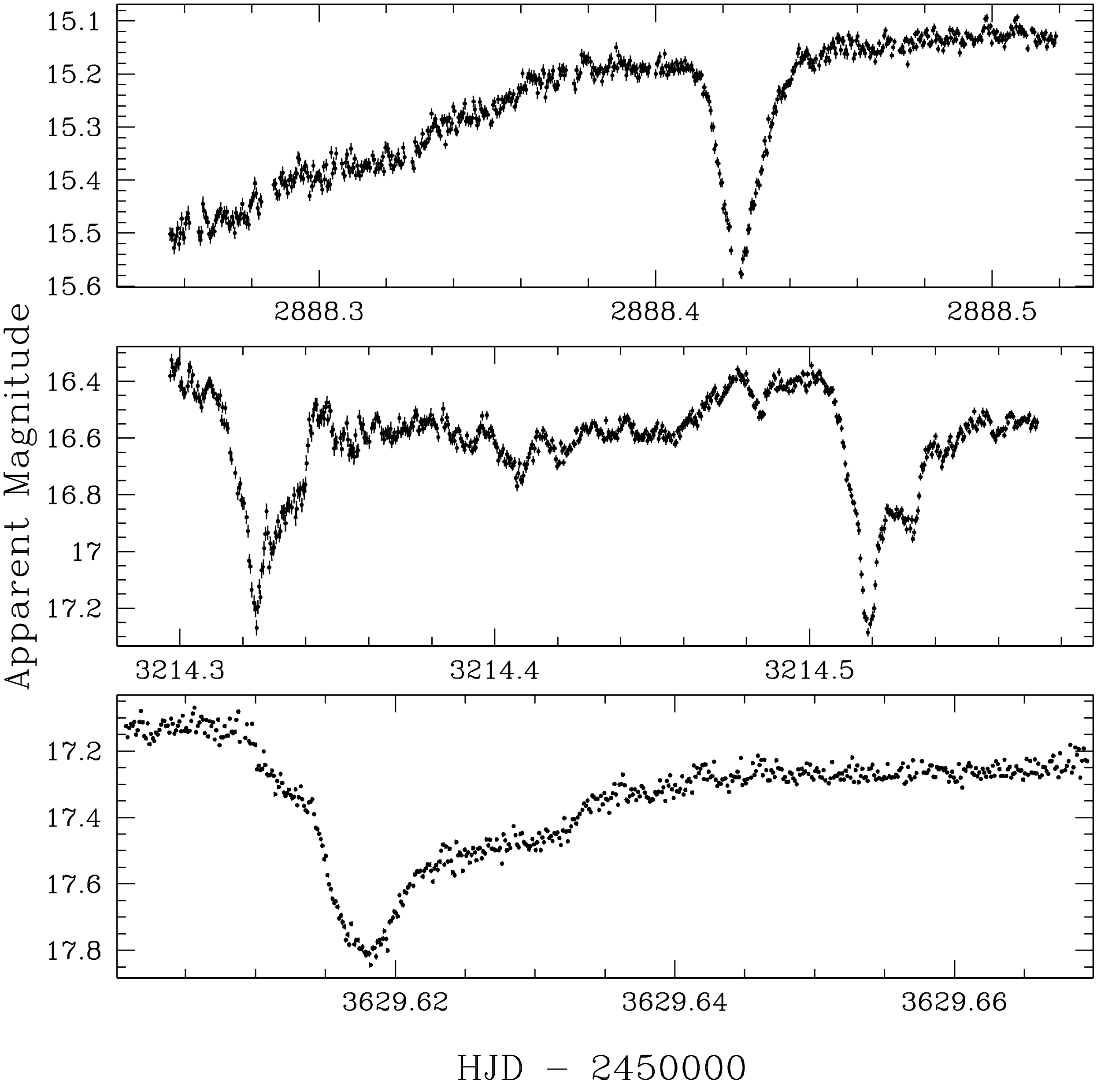

Fig. 1.— Sample light curves of HS 2325. Top panel: filterless KY observations, from September 5, 2003 (ID01), with the system on the rise to outburst. Middle panel: filterless KY observations, from July 27, 2004 (ID06), with the system in an intermediate state, Bottom panel: filterless NOT observations, from September 15, 2005 (ID13), with the system in quiescence.

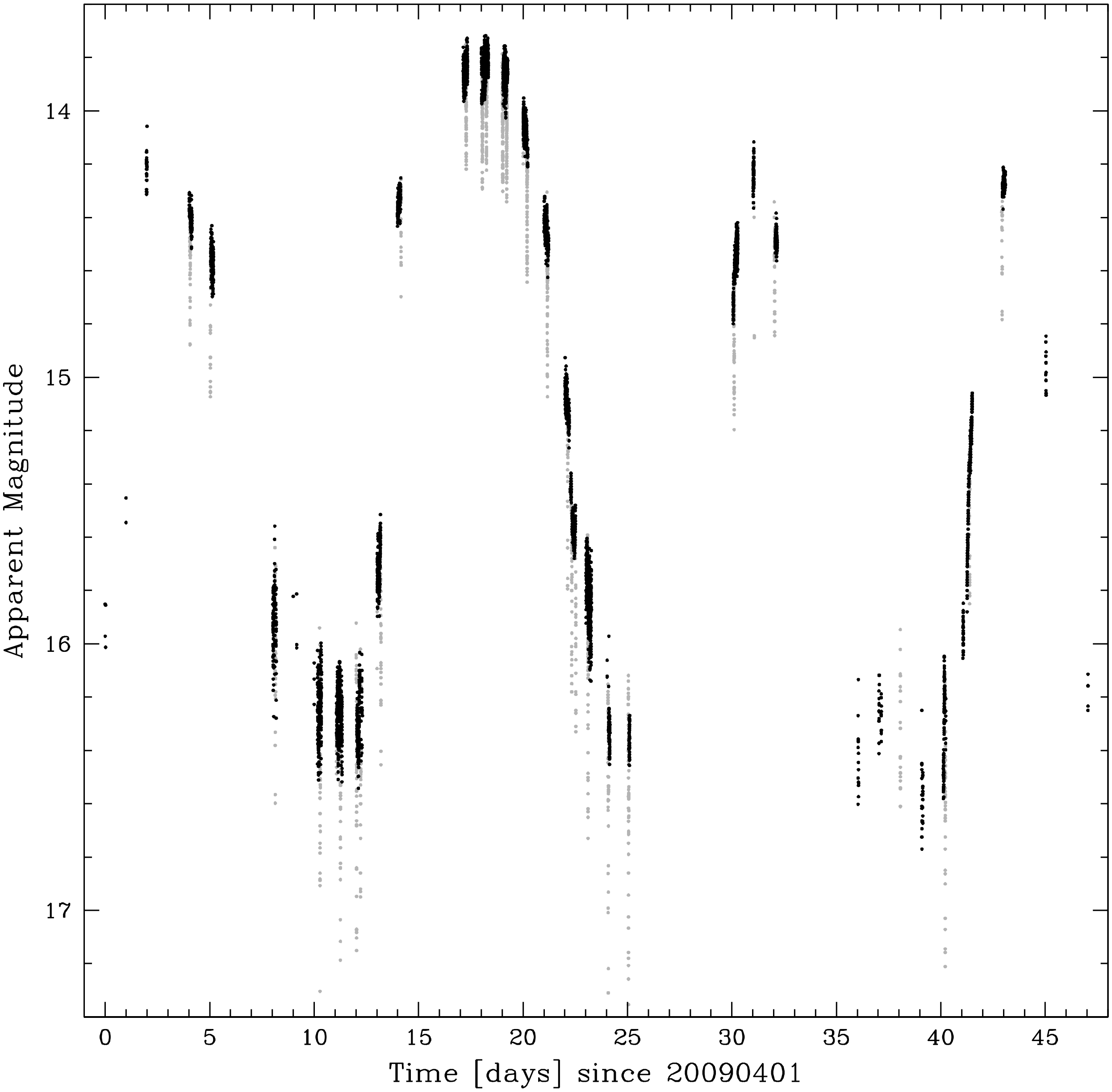

Fig. 2.— The result of the outburst monitoring campaign for HS 2325. Four outbursts have been recorded in 50 days. Points in light grey indicate the system being in eclipse.

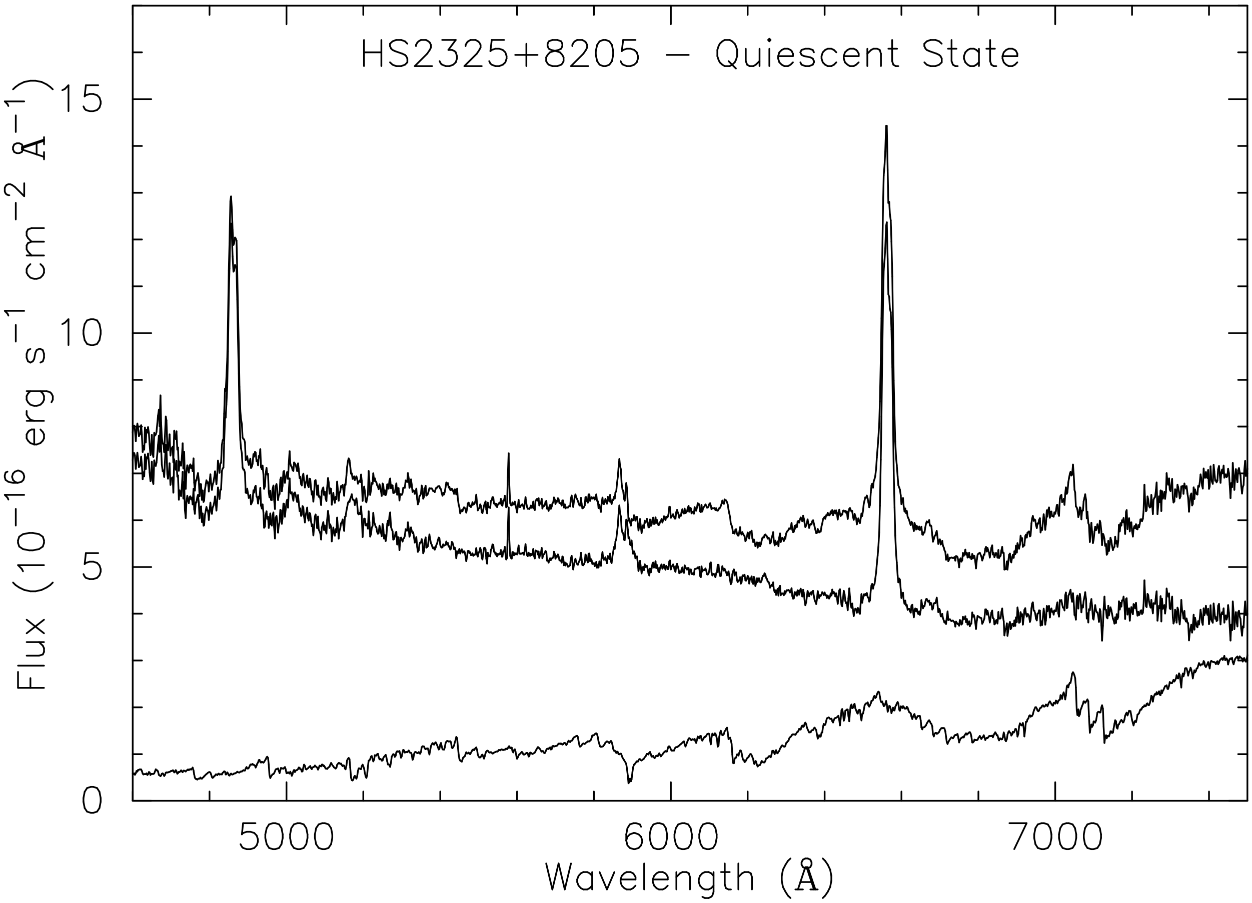

Fig. 3.— Top trace: Mean quiescent spectrum of HS 2325. Bottom trace: A library spectrum of the M3 dwarf Gliese 436, scaled so that it has an apparent V-band magnitude of $\sim$ 19.0. Middle trace: The HS 2325 spectrum minus the scaled M-dwarf.

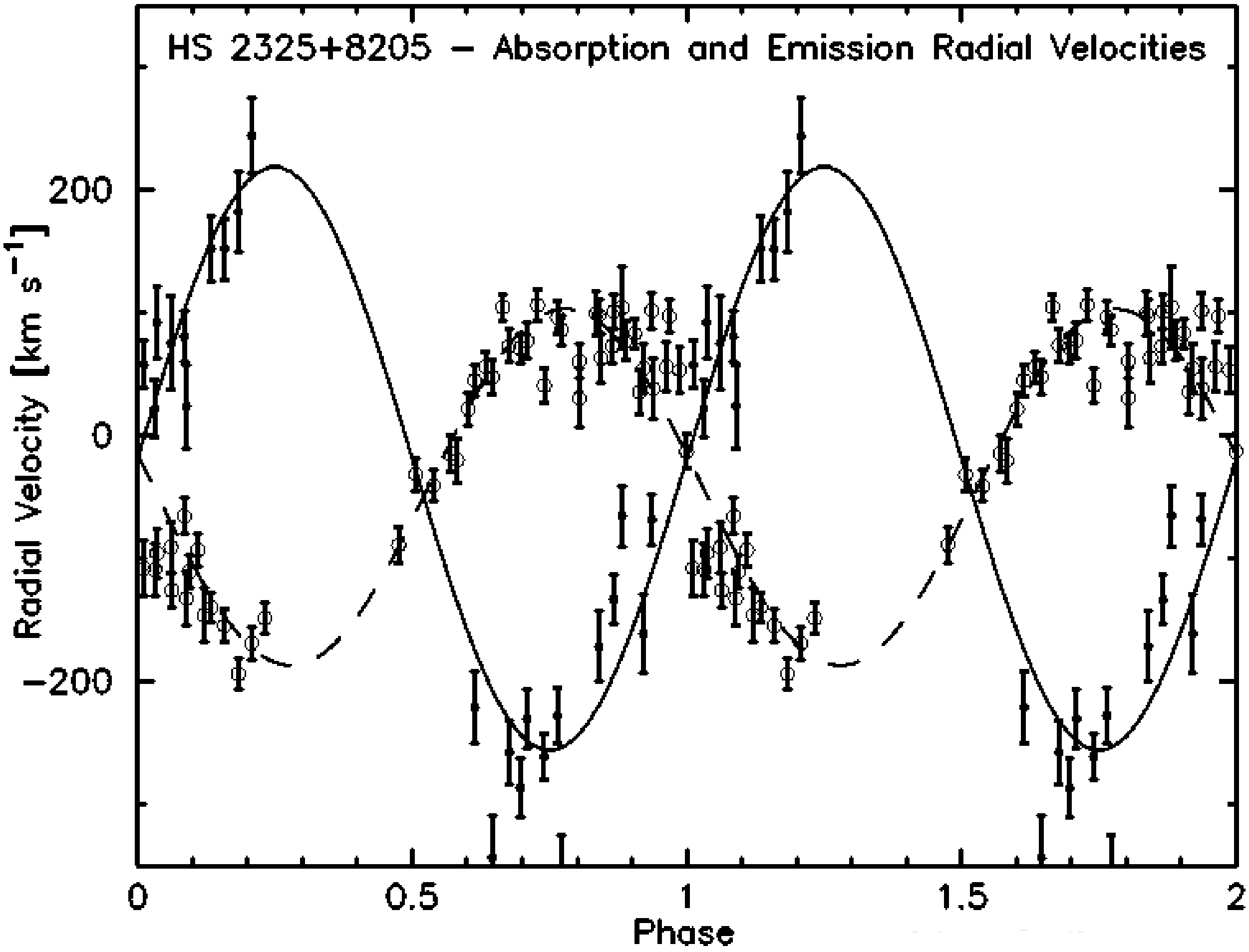

Fig. 4.— Radial velocities of HS 2325 in the quiescent state, plotted as a function of orbital phase. The open circles show the Hα emission and their formal uncertainties, and the solid dots show the cross-correlation velocities of the M dwarf. There is a gap in coverage at $0.25 < \phi < 0.42$, and only some of the spectra yielded usable absorption velocities. The dashed curve shows the best fit to the emission velocities, with $P_{\rm orb}$ fixed but T_0, K, and γ allowed to vary. For the absorption velocity fit (solid line), the T_0 was held fixed to the eclipse phase, K and γ were adjusted.

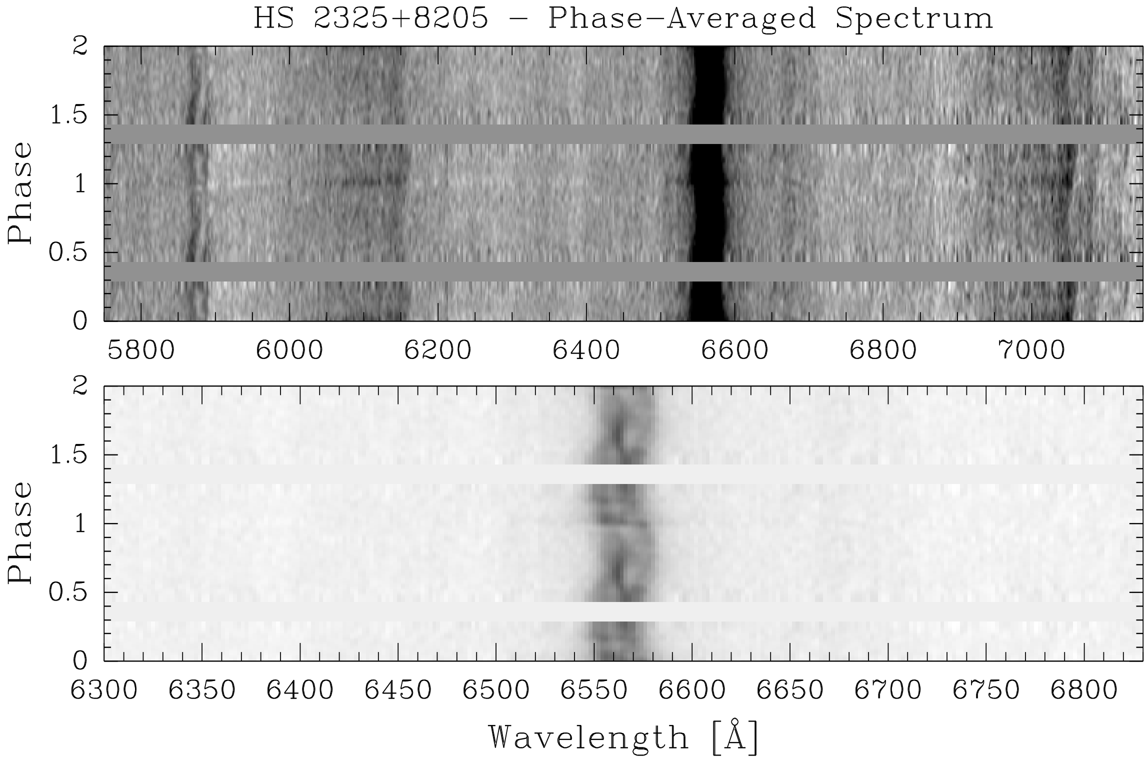

Fig. 5.— Greyscale representation of the low-state spectra, presented as a function of orbital phase. The data are repeated for a cycle to preserve continuity. The two panels show the same data, but differ in the choice of greyscale limits. The horizontal blank bars are holes in the phase coverage. To create the figure the spectra were first rectified and cleaned of remaining cosmic ray hits; each line of the figure is a weighted average of spectra nearby in phase to the line's nominal phase, the weights being computed using a narrow gaussian.

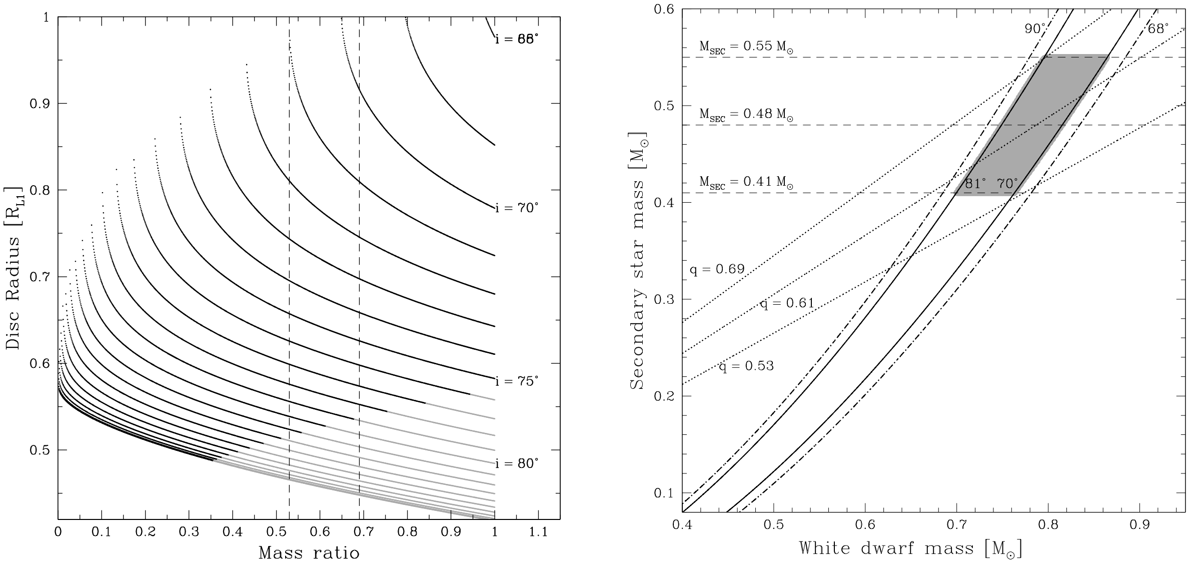

Fig. 6.— Left panel: Accretion disc radius, in units of $[R_{L_1}]$, as a function of q and i; the curves are bound below - grey coloured - by the requirement of a partial disc eclipse, while the vertical dashed lines correspond to a spectroscopic constraint on q (see text for details). Right panel: constraints on the masses of the binary components; Eq. 2 plotted for $i = 68°, 90°$ (dash-dot curves) and $i = 70°, 81°$ (solid curves), constraints on the secondary mass assuming the mass-period relation of Smith & Dhillon (1998) (dashed lines) and constraints on the mass ratio q assuming $K_{\rm em} = K_{\rm WD}$ (dotted lines). Shaded in grey is the allowed parameter space, under the previous assumptions (see text for details).